Influence of the binder types on the electrochemical characteristics of natural graphite electrode in room-temperature ionic liquid

Koichi Ui [a,*], Jun Towada [a], Sho Agatsuma [a], Naoaki Kumagai [a], Keigo Yamamoto [b], Hiroshi Haruyama [b], Ken Takeuchi [c], Nobuyuki Koura [b]

[a] Department of Frontier Materials and Functional Engineering, Graduate School of Engineering, Iwate University, 4-3-5 Ueda, Morioka, Iwate 020-8551, Japan
[b] Faculty of Science and Technology, Tokyo University of Science, Noda, Chiba 278-8510, Japan
[c] Faculty of Industrial Science and Technology, Tokyo University of Science, Tomino, Oshamanbe 049-3514, Japan

ARTICLE INFO

ABSTRACT

To improve the electrochemical characteristics of the natural graphite (NG-3) negative electrode in the LiCl saturated AlCl$_3$-1-ethyl-3-methylimizadolium chloride + thionyl chloride (SOCl$_2$) melt as the electrolyte for non-flammable lithium-ion batteries, we examined the influence of the binder types on its electrochemical characteristics. The cyclic voltammograms showed that the reduction current at 1.2–3.2 V vs. Li/Li(I) was repressed using polyacrylic acid (PAA) as the binder. The charge–discharge tests showed that the discharge capacity and the charge–discharge efficiency of the NG-3 electrode coated with the PAA binder at the 1st cycle were 322.8 mAh g^{-1} and 65.6%, respectively. Compared with the NG-3 electrode using the conventional poly(vinylidene fluoride) binder, it showed considerably a better cyclability with the discharge capacity of 302.1 mAh g^{-1} at the 50th cycle. Li(I) ion intercalation into the graphite layers could be improved because the NG-3 electrode coated with the PAA binder changed to a golden-yellow color after the 1st charging, and the formation of first stage LiC$_6$ was demonstrated by X-ray diffraction (XRD) measurement. In addition, the XRD and X-ray photoelectron spectroscopy indicated that one of the side reactions during charging was the formation of LiCl on the graphite surface regardless of the binder types.

© 2010 Elsevier B.V. All rights reserved.

1. Introduction

In recent years, an attempt has been made to use lithium-ion secondary batteries as automotive power supplies and as an electric energy storage system for grid-connection with new energy resources, but an enhancement of the energy density is still necessary. Further improvement of its safety is also necessary because there have been ignition accidents of lithium-ion secondary batteries. Therefore, novel electrolytes and electrode materials are being widely developed. Especially, room-temperature ionic liquids (RTILs) as novel electrolytes have recently been investigated because they have the advantages of a low volatility and non-flammability.

However, the charge–discharge characteristics of a graphite negative electrode in many types of RTILs are poor. This would be due to the electrochemical organic cation intercalation into the graphite layers [1,2] before the formation of a solid electrolyte interface (SEI) film on the graphite particles during the 1st charging.

Recently, it has been reported that the graphite electrode indicated good charge–discharge characteristics by adding an additive such as vinylene carbonate [3] to the RTILs or using the RTILs such as N,N-diethyl-N-methyl-N-(2-methoxyethyl) ammonium bis(trifluoromethylsulfonyl) amide (DEME-TFSA) [4], 1-ethyl-3-methylimizadolium bis(fluorosulfonyl) amide (EMI-FSA) [5], and N-methyl-N-propylpyrrolidinium bis(fluorosulfonyl) amide (P$_{13}$-FSA) [6].

On the other hand, our group found that polyacrylic acid (PAA), which is a water-soluble polymer, was able to be used as the binder of the graphite electrode [7]. In a propylene carbonate (PC)-based electrolyte, electrochemical Li$^+$ ion intercalation into graphite layers does not occur due to the co-intercalation and significantly reductive decomposition of PC molecules at around 1.0 V vs. Li/Li$^+$, causing exfoliation of the graphite layers [8]. It is expected that the charge–discharge reaction of the graphite electrode would be improved in RTILs because the uses of PC-based electrolyte and PAA binder enabled the reaction [7]. We have investigated the property of the electrolyte consisting of the AlCl$_3$-1-ethyl-3-methyl imidazolium chloride (EMIC) melt, because the 60.0 mol% AlCl$_3$–40.0 mol% EMIC–LiCl$_{sat.}$ + 0.1 mol dm^{-3} thionyl chloride (SOCl$_2$) melt exhibiting relatively good physical proper-

ties such as a low viscosity (23.4 mPa s at 25 °C) and high ionic conductivity (11.5 mS cm^{-1} at 25 °C) [9–12], and showed that the binder-free natural graphite electrode exhibited charge–discharge reaction in the melt [13,14]. The nearly reversible intercalation and deintercalation reactions of the Li(I) ions into and from the graphite layer were enabled by adding the small amount of SOCl$_2$ to the melt although the initial cycling efficiency was not high.

In this study, we tried to improve the electrochemical characteristics of the natural graphite negative electrode in the 66.7 mol% AlCl$_3$–33.3 mol% EMIC–LiCl$_{sat.}$ + 0.1 mol dm^{-3} SOCl$_2$ melt. We will report the influence of the binder types on the graphite electrode using PAA as the binder, especially compared to the conventional poly(vinylidene fluoride) (PVdF) binder. The aims of this study are to understand the formation mechanism of surface film on graphite electrodes and then to prepare the graphite electrode showing the reversible Li(I) ion intercalation and deintercalation reaction in the RTILs.

2. Experimental

The natural graphite (Kansai Coke and Chemical Co. NG-3) electrodes coated with the PAA binder and PVdF binder were prepared in a similar way as previously reported [7]. In order to improve the dispersion state of the NG-3 particles and the electrochemical stability of the electrode, the graphite electrodes were prepared as follows. The suspension composed of 90 wt.% NG-3 powder and 10 wt.% binder was prepared using a disperse medium, and then stirred in a reagent bottle for 24 h. The percentages by mass of the electrode material in the suspension for the PAA-NG-3 suspension (distilled water as disperse medium) and the PVdF-NG-3 suspension (N-methylpyrrolidone as disperse medium) were 20.0 wt.% and 43.5 wt.%, respectively. The suspension was coated on Ni mesh (Tokyo Screen Co., 100 mesh, 10 mm × 10 mm). It was then pressed for 10 min after air-drying at 80 °C for 1 h. Prior to their use, the PAA-NG-3 electrode and the PVdF-NG-3 electrode were dried in a vacuum at 200 °C and 180 °C for 3 h, respectively.

The three-electrode cell, which consisted of the NG-3 electrode (W.E.) and a pressed lithium metal foil on the Ni mesh (R.E. and C.E.), was used for the electrochemical measurements. The 66.7 mol% AlCl$_3$–33.3 mol% EMIC–LiCl$_{sat.}$ + 0.1 mol dm^{-3} SOCl$_2$ melt was prepared as previously reported [14,15]. The cells were assembled in a glove box (Miwa Mtg Co., Ltd., DBO-1NKP-1V-2) filled with dry argon at room temperature.

Cyclic voltammetry (CV) was performed using a computer-controlled electrochemical measuring system (Hokuto Denko, HZ-5000). The cyclic voltammograms were measured at the scan rate of 0.1 mV s^{-1} between the potentials of 0.0 and 2.0 V (vs. Li/Li(I)). Hereafter all the potentials described are with regard to "vs. Li/Li(I)" unless otherwise noted. The charge–discharge cycle tests were performed using an automatic battery charging-discharging instrument (Hokuto Denko, HJR-1010mSM8) at the current density of 175 mA g^{-1} (1C = 350 mA g^{-1}) between 5 mV and 2.0 V. Especially, the charge condition was controlled using the relationship between the potential and the time: the charge process was stopped when the charge potential reached down to 5 mV or the charge time reached to 3 h. The crystal structure and surface analysis of the samples were examined by X-ray diffraction (XRD) using an X-ray diffractometer (Rigaku Denki, RINT2200) with Cu Kα radiation (λ = 0.15418 nm) and tube voltage/tube current at 40 kV/30 mA, and X-ray photoelectron spectroscopy (XPS) analysis (Perkin-Elmer, PHI 5600) with Al Kα radiation (hν = 1486 eV). The cells were disassembled in the glove box to obtain the electrode samples. The obtained samples were then washed with diethyl carbonate (Wako Chemical Industries, Ltd., superfire quality), and packaged
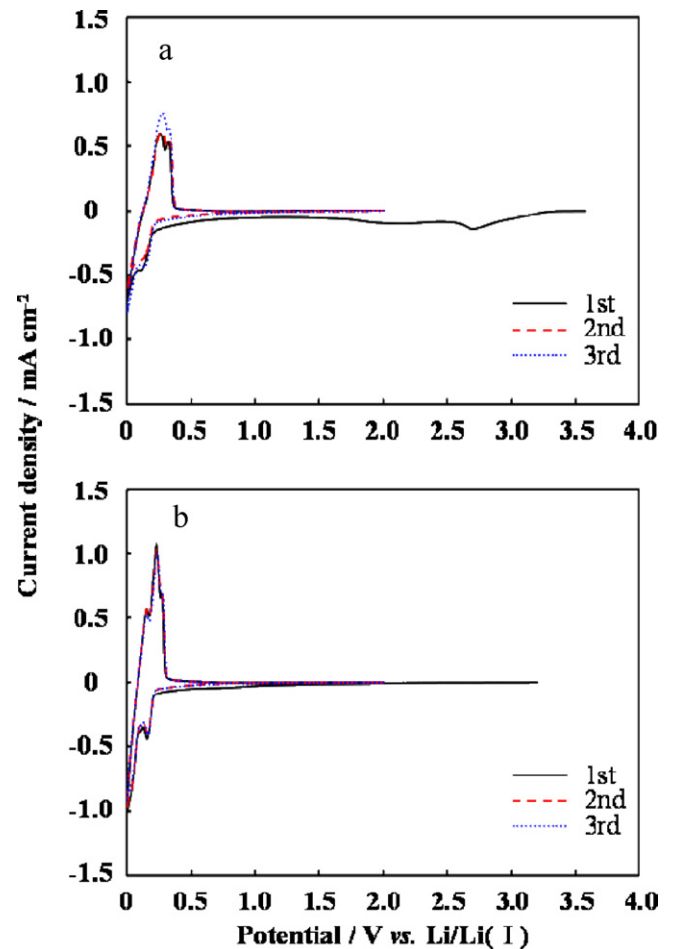

Fig. 1. Cyclic voltammograms of NG-3 electrodes coated with PVdF and PAA as a binder in the 66.7 mol% AlCl$_3$–33.3 mol% EMIC–LiCl$_{sat.}$ + 0.1 mol dm^{-3} SOCl$_2$ electrolyte. Scan rate: 0.1 mV s^{-1}; (a) PVdF 10 wt.% and (b) PAA 10 wt.%.

in polypropylene film (Rigaku Denki, Cell sheet) to prevent any contact of the sample with air.

3. Results and discussion

The CVs were measured in order to investigate the electrochemical behavior of the NG-3 electrodes in the 66.7 mol% AlCl$_3$–33.3 mol% EMIC–LiCl$_{sat.}$ + 0.1 mol dm^{-3} SOCl$_2$ melt. Fig. 1(a) shows the CV of the NG-3 electrode using PVdF (10 wt.%) as a conventional binder. The clear reduction current was observed around 2.8 V (vs. Li/Li(I)), which might be due to the reduction of SOCl$_2$ [16]. The small reduction current continuously appeared by scanning to a lower potential down to 0.2 V. The reduction and oxidation currents corresponding to the intercalation and deintercalation reactions of the Li(I) ions into and from the graphite layer were observed in the potential range from 0.2 to 0.0 V and from 0.1 to 0.4 V, respectively [17], indicating that the reversible charge–discharge reaction of the NG-3 electrode would occur in the melt. In contrast, Fig. 1(b) shows the CV of the NG-3 electrode coated with PAA (10 wt.%) as a binder. The reduction wave around 2.8 V, which was observed in the PVdF binder (Fig. 1(a)), hardly appeared during the 1st cycle. The reduction wave at 3.0–0.2 V for the NG-3 electrode coated with the PAA binder was smaller than that for the NG-3 electrode using the PVdF binder. The redox peaks corresponding to the Li(I) ion intercalation/deintercalation also appeared in the potential range from 0.2 V to 0 V. The results suggested that the irreversible reduction
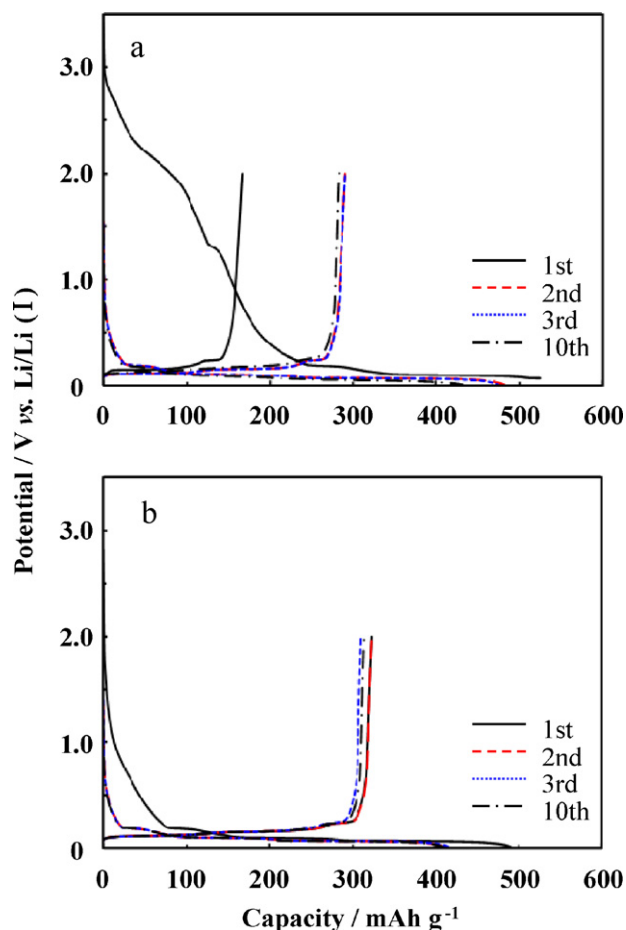
Fig. 2. Charge–discharge curves of NG-3 electrodes coated with PVdF and PAA as the binder in the 66.7 mol% AlCl$_3$–33.3 mol% EMIC–LiCl$_{sat.}$ + 0.1 mol dm^{-3} SOCl$_2$ electrolyte; C.D., 175 mA g^{-1} (0.5 C); (a) PVdF 10 wt.% and (b) PAA 10 wt.%.

Fig. 3. Cycle performance of NG-3 electrodes coated with PVdF and PAA as the binder in the 66.7 mol% AlCl$_3$–33.3 mol% EMIC–LiCl$_{sat.}$ + 0.1 mol dm^{-3} SOCl$_2$ electrolyte; potential range: 5 mV to 2.0 V vs. Li/Li(I), C.D., 175 mA g^{-1} (0.5 C); (a) PVdF 10 wt.% and (b) PAA 10 wt.%; (○) discharge capacity; (●) charge–discharge efficiency.

current of the NG-3 electrode in the melt was repressed using PAA as the binder.

Fig. 2 shows the charge–discharge curves of the NG-3 electrodes at a constant current density of 175 mA g^{-1} (0.5 C). In this paper, the cathodic polarization due to the Li(I) ion intercalation into the graphite layer is defined as a charge and the anodic polarization due to the Li(I) ion deintercalation is defined as a discharge. The charge–discharge curves of the NG-3 electrode using PVdF as the binder are shown in Fig. 2(a). The discharge capacity and the charge–discharge efficiency at the 1st
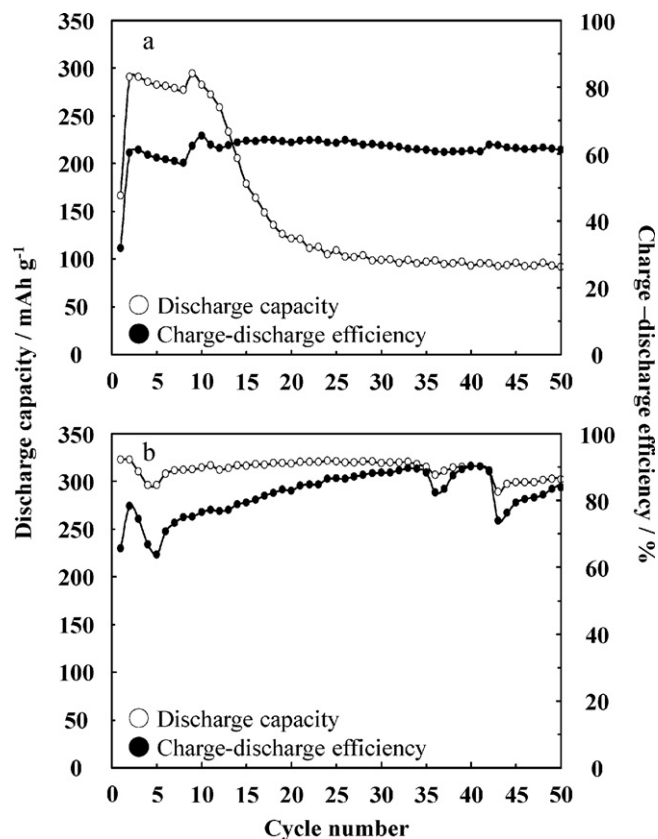
cycle were 166.5 mAh g^{-1} and 31.7%, respectively. The discharge capacity and the charge–discharge efficiency at the 2nd cycle were 290.9 mAh g^{-1} and 60.4%, respectively. The potential plateaus appeared at almost the same potential as the reduction wave of ca. 2.8 V observed in the CV (Fig. 1(a)) during the 1st charge, which might be due to the reduction of SOCl$_2$ [16]. In addition, the initial charge–discharge profile of the NG-3 electrode using PVdF as a binder was very similar to that of the binder-free natural graphite electrode, and the charge–discharge efficiency of the binder-free natural graphite at the 1st cycle (37.3%) was close to that of the electrode using the PVdF binder (31.7%) [14], indicating that the presence of the PVdF binder has little influence on the
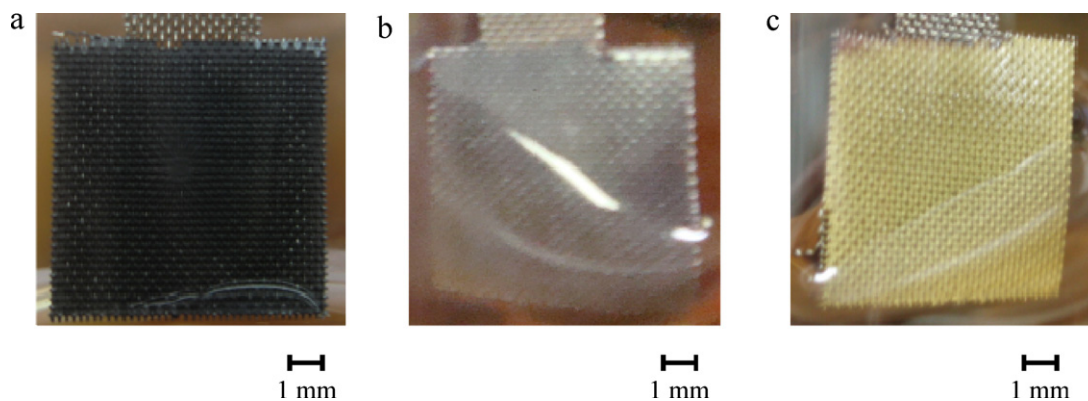

Fig. 4. Photograph of NG-3 electrodes coated with PVdF and PAA as the binder before and after charging down to 5 mV vs. Li/Li(I) in the 66.7 mol% AlCl$_3$–33.3 mol% EMIC–LiCl$_{sat.}$ + 0.1 mol dm^{-3} SOCl$_2$ electrolyte; (a) PAA 10 wt.% before charging (b) PVdF 10 wt.% after charging and (c) PAA 10 wt.% after charging.

electrochemical characteristics of the natural graphite electrode. In contrast, the charge–discharge curves of the NG-3 electrode coated with PAA as a binder are shown in Fig. 2(b). The discharge capacity and the charge–discharge efficiency at the 1st cycle were 322.8 mAh g^{-1} and 65.6%, respectively. The discharge capacity and the charge–discharge efficiency at the 2nd cycle were 322.7 mAh g^{-1} and 78.3%, respectively. After initial 2 cyclings, the charge–discharge curves were stabilized. Especially, the potential plateaus between 1.0 V and 3.0 V, which were observed in the case of the NG-3 electrode using the PVdF binder, were not observed as suggested from the CV (Fig. 1(b)). Based on these results, the first point to note is that the PAA binder can effectively improve the initial electrochemical characteristics of the NG-3 electrode.

Fig. 3 indicates the cycle performance of the NG-3 electrodes. The cycle performance and the charge–discharge efficiency of the NG-3 electrode using PVdF as a binder are shown in Fig. 3(a). Although the reversible discharge capacity was maintained at ca. 300 mAh g^{-1} from the 2nd cycle to the 10th cycle, it rapidly faded after the 11th cycle. The discharge capacity at the 50th cycle decreased to 91.6 mAh g^{-1}. In contrast, the cycle performance and the charge–discharge efficiency of the NG-3 electrode coated with PAA as a binder are shown in Fig. 3(b). During 50 cyclings, the reversible discharge capacity was rather constant and the charge–discharge efficiency was maintained at around 80%. The discharge capacity and the charge–discharge efficiency at the 50th cycle were 302.1 mAh g^{-1} and 83.9%, respectively. Based on these results, more noteworthy is that the NG-3 electrode coated with the PAA binder showed a better cycle performance. It is considered that the significant capacity fade in the NG-3 electrode using the PVdF binder would be caused by the electrochemical local isolation of the particles as will be described later.

The surface of the NG-3 electrode before and after charging was observed (Fig. 4). Fig. 4(a) is a close-up photograph of the NG-3 electrode coated with the PAA binder before charging. As seen in the photo, the surface of the graphite electrode was black. The surface of the NG-3 electrode using the PVdF binder was the same as that coated with the PAA binder. Fig. 4(b) is a photograph of the NG-3 electrode using the PVdF binder after charging down to 5 mV. As seen in the photo (b), the surface of the graphite electrode changed to gray, indicating that the 1st stage LiC$_6$ would not be formed by the Li(I) ion intercalation into graphite layers during charging. In contrast, Fig. 4(c) is a photograph of the NG-3 electrode coated with the PAA binder after charging down to 5 mV. As seen in the photo(c), the surface of the graphite electrode after charging changed to a golden-yellow color. This indicates that the 1st stage LiC$_6$ would be formed during charging [17]. However, the both surfaces of the NG-3 electrodes (b and c) became black after discharging up to 2.0 V, suggesting that the electrochemical intercalation of the Li(I) ion in the NG-3 electrode occurred in a reversible manner in the melt.

The *ex situ* XRD patterns were measured in order to investigate the structural change in the NG-3 electrode during the 1st charge–discharge. Fig. 5(a) indicates the *ex situ* XRD patterns of the NG-3 electrode using the PVdF binder. The (002) and (004) peaks observed at 26.4° (d = 338 pm) and 54.6° (d = 168 pm), respectively, were ascribed to the diffraction peaks of the natural graphite before charging. The diffraction peaks of the natural graphite shifted to the lower positions of 24.1° (d = 370 pm) and 49.3° (d = 185 pm) corresponding to (0 0 1) and (0 0 2), respectively, after charging down to 5 mV. This indicates that the distance between the graphite layers increased due to the Li(I) ion intercalation after charging. These values correspond to the formation of the stage 1 intercalation compound, LiC$_6$. However, as has been pointed out in Fig. 4, the amount of the LiC$_6$ formed would be very small. After charging down to 5 mV, the peaks of LiC$_6$ were detected as only small peak, indicating that a small amount of LiC$_6$ phase would be formed after charging. This XRD pattern corresponds to the close-up pho-
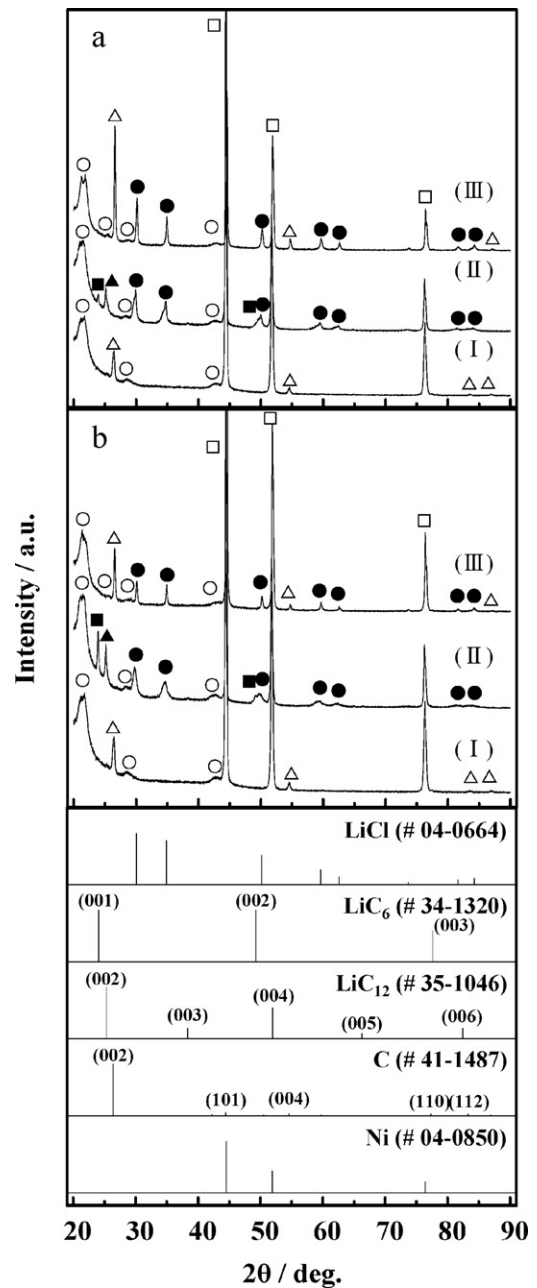

Fig. 5. *Ex situ* XRD patterns of NG-3 electrodes coated with PVdF and PAA as the binder in the 66.7 mol% AlCl$_3$−33.3 mol% EMIC–LiCl$_{sat.}$ + 0.1 mol dm^{-3} SOCl$_2$ electrolyte; (a) PVdF 10 wt.%, (b) PAA 10 wt.%; (●) LiCl; (■) LiC$_6$; (▲) LiC$_{12}$; (△) C; (□) Ni(sub.); (○) polypropylene film. In both cases, X-ray diffractions were taken (I) before charging (II), after charging down to 5 mV *vs.* Li/Li(I), and (III) discharging up to 2.0 V *vs.* Li/Li(I).

tograph of Fig. 4(b). It seems reasonable to suggest that the Li(I) ion intercalation into the graphite layers could not totally occur because the strain of the graphite layer would be increased and then the particles would become electrochemically isolated by the local exfoliation of graphite layer due to the formation of LiC$_{12}$ [18]. In the case of the PAA binder, the stack of the electrochemical local isolation may be repressed physically and mechanically because the graphite particles would coat with it more completely. Therefore, the surface of the NG-3 electrode using the PVdF binder after charging did not change to a golden-yellow color, as shown in Fig. 4(b). After discharging, however, the peaks of LiC$_{12}$ disappeared and the structure of graphite was almost recovered. In contrast, the *ex situ* XRD patterns of the NG-3 electrode coated with the PAA binder are
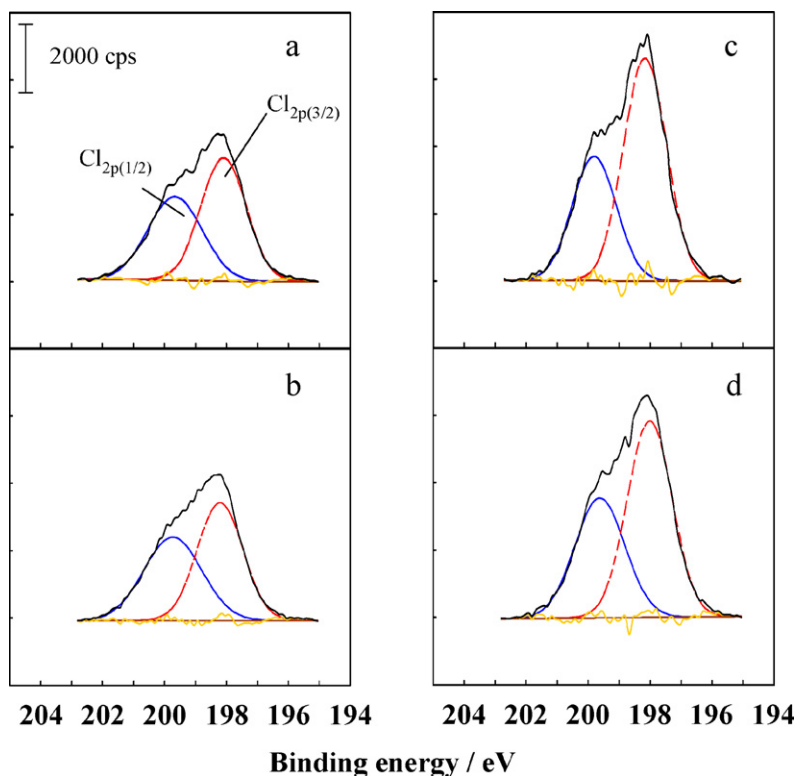
Fig. 6. High resolution XPS spectra of Cl_{2p} region for NG-3 electrodes coated with PVdF and PAA as the binder in the 66.7 mol%AlCl$_3$–33.3 mol% EMIC–LiCl$_{sat.}$ + 0.1 mol dm^{-3} SOCl$_2$ electrolyte; (a) PVdF 10 wt.% after charging down to 5 mV *vs.* Li/Li(I), (b) PVdF 10 wt.% discharging up to 2.0 V *vs.* Li/Li(I). (c) PAA 10 wt.% after charging down to 5 mV *vs.* Li/Li(I), (d) PAA 10 wt.% discharging up to 2.0 V *vs.* Li/Li(I).

shown in Fig. 5(b). The peaks of LiC$_{12}$ and LiC$_6$ appeared similar to those of the NG-3 electrode using the PVdF binder after charging. The peak intensity of LiC$_6$ is higher in comparison to that of the NG-3 electrode using the PVdF binder, and the formation of the LiC$_6$ phase was obviously observed at $2\theta = 24.1°$ and $49.3°$. This may be due to the reinforcement with an extra connection by the esterification between hydroxyls on edge of the graphite and the carboxyls in the PAA [19]. As a result, it is suggested that the irreversible reduction of SOCl$_2$ would be repressed because PAA acted as an organic layer for the quasi-SEI film effectively. Based on the results, it was found that PAA was more effective as a binder.

Moreover, it is interesting to note that the peaks of LiCl were obviously observed on the graphite surface after charging regardless of the binder types (Fig. 5(aI) and (bI)). As LiCl was more clearly detected after discharging, it is found that it remained on the graphite surface (Fig. 5(aI) and (bI)). As shown in Fig. 5(aI) and (bI), LiCl was not formed on the graphite surface during immersing the graphite electrodes in the melt or before charging. Furthermore, the XPS measurements showed that Cl$^-$ ions were included in the surface film on the graphite electrodes after charging and discharging (Fig. 6). The two XPS peaks can be ascribed to the formation of LiCl, because these binding energies almost correspond to the literature values (Cl$_{2p1/2}$ (199.5 eV) and Cl$_{2p3/2}$ (197.5 eV)) [20,21]. The main ionic species in the melt were thought to be EMI$^+$, Li(I), and AlCl$_4^-$ [11]. Thus, it is assumed that the AlCl$_4^-$ ion is reduced electrochemically, resulting in the formation of LiCl at -1.4 V *vs.* Al/Al(III) (= 0.8 V *vs.* Li/Li(I), [15]) according to Eq. (1) [2].

$$AlCl_4^- + 4Li(I) + 3e^- \rightarrow Al(s) + 4LiCl(s) \tag{1}$$
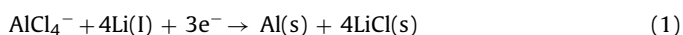
In the case of several RTILs, several researches on the electrochemical reduction of the AlCl$_4^-$ and (CF$_3$SO$_2$)$_2$N$^-$ have been reported [2,22]. Based on the results, it was considered that the PAA binder would not repress the reduction reaction of AlCl$_4^-$ at

0–1.0 V although it would effectively repress the reduction reaction of SOCl$_2$ at 1.2–3.2 V.

4. Conclusions

We tried to improve the electrochemical characteristics of the natural graphite negative electrode in the 66.7 mol% AlCl$_3$–33.3 mol% EMIC–LiCl$_{sat.}$ + 0.1 mol dm^{-3} SOCl$_2$ melt. The use of the PAA binder enabled to improve its capacity retention and the initial cycling efficiency of the NG-3 electrode. Especially, the intercalation and deintercalation reactions of the Li(I) ion into and from the graphite layer were enhanced in a reversible manner because the reduction reaction derived from SOCl$_2$ would be repressed. It was suggested that the main side reaction of Eq. (1) during charging would be the formation of LiCl on the graphite surface regardless of the binder types.

This study is the first report concerning the characterization of the deposit, like the inorganic components in the SEI film, on the natural graphite electrode in the RTILs electrolyte.

References

[1] R.T. Carlin, H.C. De Long, J. Fuller, P.C. Trulove, J. Electrochem. Soc. 141 (1994) L73.
[2] R.T. Carlin, J. Fuller, W.K. Kuhn, M.J. Lysaght, P.C. Trulove, J. Appl. Electrochem. 26 (1996) 1147.
[3] H. Zheng, K. Jiang, T. Abe, Z. Ogumi, Carbon 44 (2006) 203.
[4] S. Seki, Y. Kobayashi, H. Miyashiro, Y. Ohno, Y. Mita, A. Usami, N. Terada, M. Watanabe, Electrochem. Solid-State Lett. 8 (2005) A577.

[5] M. Ishikawa, T. Sugimoto, M. Kikuta, E. Ishiko, M. Kono, J. Power Sources 162 (2006) 658.
[6] S. Seki, Y. Kobayashi, H. Miyashiro, Y. Ohno, Y. Mita, N. Terada, P. Charest, A. Guerfi, K. Zaghib, J. Phys. Chem. C 112 (2008) 16708.
[7] K. Ui, S. Kikuchi, F. Mikami, Y. Kadoma, N. Kumagai, J. Power Sources 173 (2007) 518.
[8] A.N. Dey, B.P. Sullivan, J. Electrochem. Soc. 117 (1970) 222.
[9] N. Koura, K. Ui, J. Jpn. Inst. Light Met. 47 (1997) 267.
[10] K. Ui, N. Koura, Y. Idemoto, K. Iizuka, Denki Kagaku 65 (1997) 161.
[11] N. Koura, K. Iizuka, Y. Idemoto, K. Ui, Electrochemistry 67 (1999) 706.
[12] K. Ui, K. Yamamoto, K. Ishikawa, T. Minami, K. Takeuchi, M. Itagaki, K. Watanabe, N. Koura, J. Power Sources 183 (2008) 347.
[13] N. Koura, K. Etoh, Y. Idemoto, F. Matsumoto, Chem. Lett. (2001) 1320.
[14] K. Ui, T. Minami, K. Ishikawa, Y. Idemoto, N. Koura, J. Power Sources 146 (2005) 698.

[15] K. Ui, K. Ishikawa, T. Furuya, Y. Idemoto, N. Koura, Electrochemistry 73 (2005) 120.
[16] J. Fuller, R.A. Osteryoung, J. Electrochem. Soc. 142 (1995) 3632.
[17] M. Letellier, F. Chevallier, M. Morerette, Carbon 45 (2007) 1025.
[18] J. Drofenik, M. Gaberscek, R. Dominko, F.W. Poulsen, M. Mongensen, S. Pejovnik, J. Jamnik, Electrochim. Acta 48 (2003) 883.
[19] N. Ding, J. Xu, Y. Yao, G. Wegner, I. Lieberwirth, C. Chen, J. Power Sources 192 (2009) 644.
[20] J.F. Moulder, W.F. Stickle, P.E. Sobol, K.D. Bomben, Handbook of X-ray Photoelectron Spectroscopy, Physical Electronics, Inc., USA, 1995, pp. 62–63.
[21] J. Arai, H. Katayama, H. Akahoshi, J. Electrochem. Soc. 149 (2002) A217.
[22] P.C. Howlett, N. Brack, A.F. Hollenkamp, M. Forsyth, D.R. MacFarlane, J. Electrochem. Soc. 153 (2006) A595.